Evaluation of performance of analytical and numerical methods to account for liquefaction effects on the seismic response of anchored quay walls

van Elsäcker, Willem; Besseling, F.; Lengkeek, Arny; Brinkgreve, Ronald; de Gijt, Jarit; Jonkman, Bas

Publication date
2017

Document Version
Accepted author manuscript

Published in
3rd International Conference on Performance-based Design in Earthquake Geotechnical Engineering

Citation (APA)
van Elsäcker, W., Besseling, F., Lengkeek, A., Brinkgreve, R., de Gijt, J., & Jonkman, B. (2017). Evaluation of performance of analytical and numerical methods to account for liquefaction effects on the seismic response of anchored quay walls. In *3rd International Conference on Performance-based Design in Earthquake Geotechnical Engineering: Vancouver, BC, Canada, from July 16-19, 2017* Article 201

Evaluation of performance of analytical and numerical methods to account for liquefaction effects on the seismic response of anchored quay walls

Elsäcker, van, W.A., Besseling, F., Lengkeek, H.J.
Witteveen+Bos Consulting Engineers, Deventer The Netherlands
Brinkgreve, R.B.J.
Delft University of Technology and PLAXIS B.V., Delft, The Netherlands
De Gijt, J.G., Jonkman, S.N.
Department of Hydraulic Engineering - Delft University of Technology, Delft, The Netherlands

ABSTRACT
Liquefaction induced by earthquakes has shown to have potential devastating influence on seismic performance of anchored quay walls. Therefore, measures to mitigate liquefaction are commonly part of the design of quay walls in seismically active regions. Such mitigation measures are costly. Moreover, these measures are difficult to implement for existing structures in operation. For these reasons, proper tools that can accurately predict the effects of liquefaction on anchored quay walls are valuable for engineering purposes. Numerical tools like finite element analysis can potentially replace simplified code based methods, such as the Mononobe-Okabe method. However, performance of numerical models that account for liquefaction and pore pressure accumulation is crucial towards the use of numerical tools for this purpose. Initial stress states influence both the liquefaction resistance of the soil as well as the performance of the constitutive model. This study proposed a new calibration procedure in order to deal with the influence of static shear and overburden stress in the model. Zones around the structure with specific corresponding stress states are defined for which the stress state dependent constitutive model behaviour is calibrated based on laboratory results and literature.This study evaluates the performance of finite element calculations with the UBC3D-PLM soil constitutive model based on a reported case study of two quay walls in Akita Port, Japan for the 1983 Nihonkai Chubu earthquake. It also evaluates to what extent Mononobe-Okabe calculations with code-based corrections for liquefaction effects could reproduce the observed performance of the Akita Port quay walls. The results shown by the analysis employing the new developed calibration procedure indicate good correspondence with observations in the field. On the other hand, Mononobe-Okabe methods including corrections for liquefaction effects give a poor fit to the observed behaviour. The response indicates that dynamic analysis with the UBC3D-PLM model using the proposed calibration procedure is capable to give insight in effects of excess pore pressures on the seismic performance of an anchored quay wall. This study mainly only focussed on liquefaction triggering as a function of stress state and the post-liquefaction stress-strain behaviour predicted by UBC3D-PLM was only evaluated at a basic level.

1 INTRODUCTION

The simplified pseudo-static Mononobe-Okabe method (Mononobe et al 1929, Okabe 1926) is often prescribed in design codes to provide seismic earth pressures on retaining structures based on the peak ground acceleration (PGA). This method was originally developed to estimate dynamic earth pressures against gravity walls, but is commonly applied in the design of anchored quay walls. Modifications to the original method that account for the effects of excess pore pressures are available and included in design codes (e.g. Eurocode 8).

The pseudo-static Mononobe-Okabe method generally yields conservative estimates of bending moments and anchor forces (Gazetas et al. 2015). Limitations of the modified method (with inclusion of excess pore pressure ratio) became evident in the evaluation of the case history of anchored quay walls at Akita Port hit by the Nihonkai Chubu Earthquake 1983 (Iai et al. 1993). Overestimation of the passive resistance and underestimation of anchor capacity led to exaggerated bending moment distributions and an overestimation of the displacements.

Numerical models can potentially replace the simplified code based methods, such as the Mononobe-Okabe method. Prediction of liquefaction is however still a challenging task and the quality of constitutive soil models that account for liquefaction and pore pressure accumulation is crucial towards the use of numerical tools for engineering purposes. Validation of well-documented case histories is of great importance in implementing these sophisticated models in design practice.

Thishis paper evaluates the performance of the effective stress UBC3D-PLM (Galavi et al. 2013) constitutive material model to account for liquefaction effects. The model is an extension of the two dimensional UBCSAND model (Puebla et al. 1997, Beaty and Byrne 1998) and is implemented in PLAXIS finite element software.

After a brief description of the constitutive model, this paper presents the effects of varying initial stress states and loading conditions on the model performance in a by

model element test. Both undrained cyclic direct simple shear (DSS) tests and undrained cyclic triaxial tests are modeled and effects of varying initial vertical effective stress (σ'_{v0}), lateral earth pressure coefficient (K_0) and initial static shear stresses (α) on modeled soil behavior are analyzed and compared with experimental laboratory data. Modifications to model parameters are required to improve the model performance for specific initial stress states, with focus on obtaining an accurate fit of the amount of cycles to liquefaction. This paper employed the well-documented case history of two anchored quay walls in Akita Port from the 1983 Nihonkai Chubu Earthquake to validate the capabilities of the UBC3D-PLM model at a global scale (Iai et al. 1993). A calibration methodology is developed to calibrate the model locally and deal with the influence of varying static shear and overburden stress around the structure. Finally a dynamic analysis with the calibrated model (as function of local stress state) is performed and numerical results are analyzed and compared to observed performance of the anchored quay walls in Akita Port.

2 UBC3D-PLM CONSTITUTIVE MODEL

The UBC3D-PLM constitutive material model uses the Mohr-Coulomb yield criterion and distinguishes a primary and secondary yield surface. The primary yield surface uses an isotropic hardening law, while the secondary yield surface evolves according to a simplified kinematic hardening rule, where the maximum reached mobilized friction angle (φ_{mob}) defines the transition between primary and secondary loading.

The elastic behaviour in the model is governed by the stress dependent elastic bulk modulus (K) and elastic shear modulus (G):

$$K = K^e_B \; P_A \; (p / p_{ref})^{me} \quad [1]$$

$$G = K^e_G \; P_A \; (p / p_{ref})^{ne} \quad [2]$$

where K^e_B and K^e_G are respectively the bulk and the shear modulus numbers at a reference stress level, P_A is the atmospheric pressure (same as p_{ref}, the reference stress level), p is the mean effective stress and me and ne define the rate of stress dependency. The model predicts elastic behaviour during unloading stage. The plastic shear strain increment is given by:

$$\delta\gamma^p = (1 / G^*) \; \delta \sin \phi_{mob} \quad [3]$$

$$G^* = K^p_G \; (p' / p)^{np} \; (1 - (\sin \varphi_{mob} / \sin \varphi_{peak}) \; R_F)^2 \quad [4]$$

in which K^p_G is the plastic shear modulus number, np is the plastic shear modulus exponent, φ_{peak} is the peak friction angle and R_F is the failure ratio. A non-associated plastic flow rule is formulated, which is based on Drucker-Prager's law (1952) and Rowe's stress dilatancy theory (1962):

$$d\varepsilon^p_v = \sin \Psi_m \; d\gamma^p \quad [5]$$

$$\sin \Psi_m = \sin \varphi_{mob} - \sin \varphi_{cv} \quad [6]$$

where $d\varepsilon^p_v$ is the volumetric strain increment, Ψ_m is the mobilized dilation angle and φ_{cv} is the phase transformation friction angle, defining contractive or dilative soil behaviour.

For the K^p_G term distinction is made between primary, secondary and post-liquefaction loading and it is described as follows:

$$K^p_G = K^p_{G,primary} \; f(n_{rev}, fac_{hard}, fac_{post}) \quad [7]$$

where $K^p_{G,primary}$ is the input value for the plastic shear modulus number, adopted during primary loading. To capture the effects of soil densification during secondary loading, the K^p_G is formulated as a function of the amount of stress reversals from loading to unloading and vice versa (n_{rev}). To calibrate the densification rule the fac_{hard} parameter is introduced to control the amount of hardening of the secondary yield surface. Larger values of fac_{hard} lead to less development of excess pore pressures and a larger liquefaction resistance, thus to a higher number of cycles to liquefaction. Once the stress path reaches the failure line, the plastic shear modulus gradually decreases as a function of the generated plastic deviatoric strain. The stiffness degradation is limited by fac_{post} value. The larger this value is, the higher the post-failure stiffness is.

3 VALIDATION OF UBC3D-PLM MODEL

3.1 Model parameters

The analysis validates the UBC3D-PLM model by comparing the results of numerically simulated element tests to experimental data. The in-situ stress conditions during dynamic loading are reproduced in direct simple shear and triaxial tests with varying initial conditions (K_0 and initial static shear) and loading conditions (axial/lateral, compression/extension). This simplified modeling still serves as a standard model for liquefaction potential evaluation (Kokusho 2015). Liquefaction resistance curves are available of both Ohama Sand and Gaiko Sand, based on undrained cyclic triaxial tests with consolidation pressure of 98 kPa performed in the laboratory (Iai et al. 1993).

Initial input model parameters for the UBC3D-PLM model are derived based on the calibration method by Beaty and Byrne (2011) and Makra (2013) and the method by Souliotis and Gerolymos (2016). Based on the measured SPT blow-count the relative density of the sand deposit is estimated according to the relationship by Skempton (1986). These initial parameter sets are calibrated by fitting the numerically obtained CSR-N_{liq} curve with liquefaction resistance curve from laboratory tests, aiming at a fit of the amount of cycles until liquefaction for a given loading condition. The input value for the plastic shear modulus number (K^p_G) and the densification factor (fac_{hard}) are adjusted since these values largely define the development of excess pore pressure, where the fac_{hard} is introduced in the model to

control the densification rule. The resulting calibrated input parameters for both Ohama Sand and Gaiko Sand are presented in Table 1.

Table 1. Calibrated input parameters UBC3D-PLM

Parameter	Unit	Ohama Sand	Gaiko Sand
φ'_{cv}	[°]	30.0	33.0
φ'_{peak}	[°]	30.9	34.0
c	kPa	0.0	1.0
k^e_B	[-]	902	934
k^p_G	[-]	319	1141
k^e_G	[-]	632	654
ne	[-]	0.50	0.50
me	[-]	0.50	0.50
np	[-]	0.40	0.40
R_f	[-]	0.7911	0.7787
p_a	kPa	100	100
σ_t	kPa	0.00	0.00
fac_{hard}	[-]	0.30	0.30
$(N1)_{60}$	[-]	9	10
fac_{post}	[-]	0.02	0.02

3.2 Evaluation of stress-path dependent liquefaction potential

Calibration of the initial model parameter set is performed based on data of undrained cyclic triaxial tests with only one initial stress state. Variation of effective overburden stress and presence of static shear stresses, however, affect the liquefaction potential of soils (Seed 1983). As was amongst others shown by Ziotopoulou, K. (2014), constitutive material models have limitations in reproducing the full range of liquefaction behaviour aspects observed in the laboratory. Simulation of the effects of initial static shear stresses is known to be one of the major challenges. Around anchored quay walls, varying initial static shear stress ratios ($\alpha = \tau_s / \sigma'_{vc}$) are present, K_0 states of soil may differ, and the effective stress increases with depth. Figure 1 depicts the contour plots of both the distribution of K_0 and α around the anchored quay wall at Ohama No.2 in Akita Port calculated in the static phase. Since the initial stress state and loading conditions influences both the liquefaction potential and the model performance. It is crucial to evaluate the performance of the constitutive model for these typical stress states using element tests.

In this section, results of numerically modeled undrained cyclic direct simple shear tests and undrained cyclic triaxial tests are presented. Liquefaction resistance curves are reproduced for different initial stress conditions (varying overburden stress, lateral earth pressure coefficient and initial static shear stress ratios) and different loading levels. Since only a limited amount of laboratory data is available, the model behavior is evaluated by comparing numerically simulated results to a combination of experimental data and empirical relationships commonly used in design practice (Seed 1983).

The evaluation of the model is intended to identify weaknesses and improve the performance of the model by targeted adjustments to the model parameters for these specific types of sand and loading conditions.

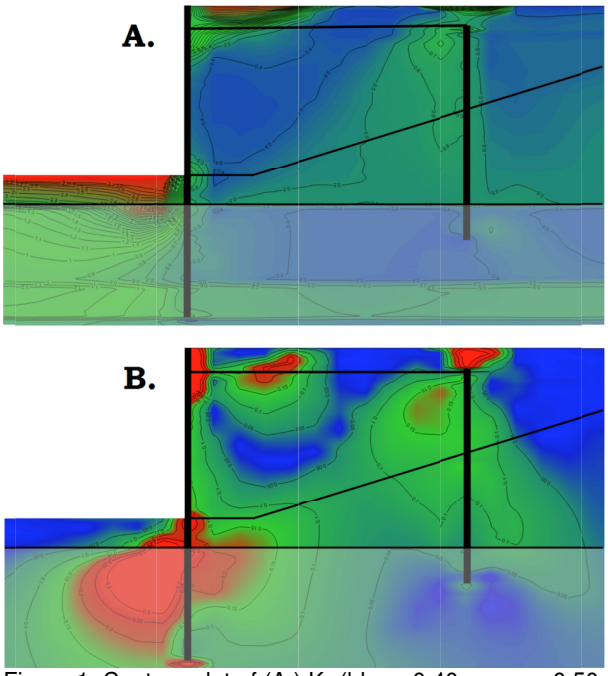

Figure 1. Contour plot of (A.) K_0 (blue - 0.40, green - 0.50, red - 2.00) and (B.) α (blue - 0.00, green - 0.10, red - 0.20) around the anchored quay wall at Ohama No.2 Wharf.

3.2.1 Effects of overburden pressure

General observation in the results of the numerical modeled element tests is that the liquefaction resistance decreases for increasing overburden stress, which is in line with empirical relationships by Seed (1983) for the types of sand presented in Table 1. The effective stress level (σ'_c) ranged from 50 kPa to 200 kPa, with a K_0 of 0.50 in in the DSS test and a K_0 of 1.0 in the TX test.

For an overburden pressure other than the reference stress level (98 kPa) the soil resistance is slightly overestimated for both undrained cyclic DSS tests and undrained cyclic triaxial tests by the model. Only for DSS loading conditions and a lower overburden stress the liquefaction resistance is underestimated. No corrections to model parameters are proposed since deviations with empirical relationships are so small.

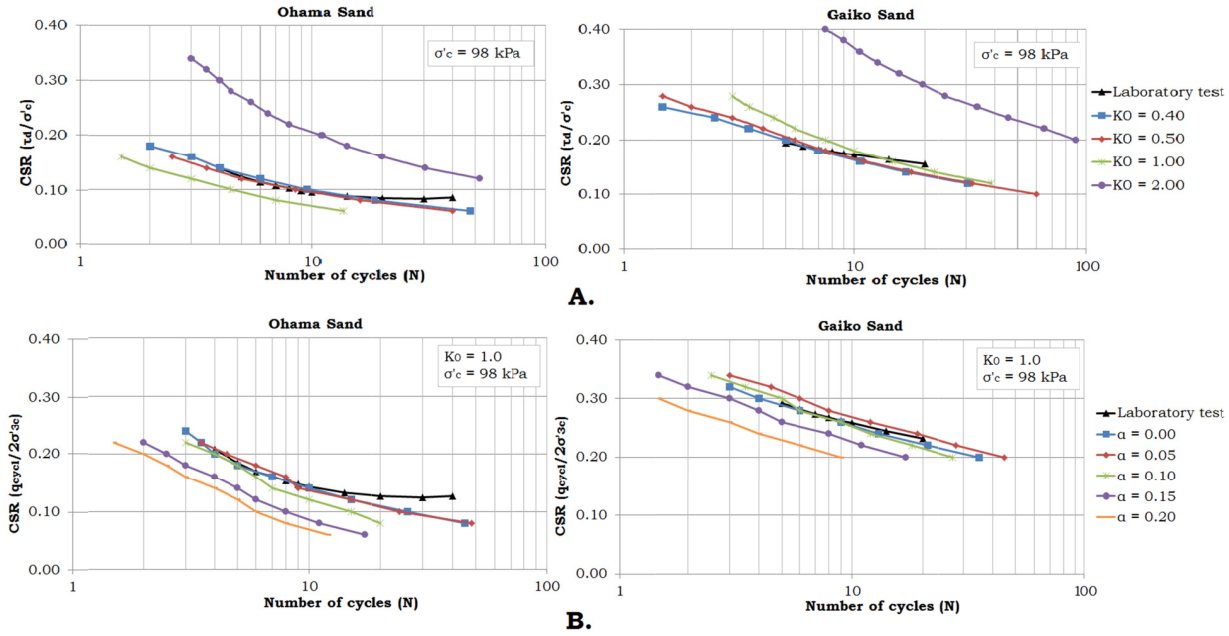

Figure 2. Prediction of the liquefaction resistance curve for (A.) undrained cyclic DSS tests with varying K_0 and (B.) undrained cyclic TX tests with varying α according to the UBC3D-PLM model with calibrated model parameter set

3.2.2 Effects of lateral earth pressure coefficient (K_0)

Figure 2(A.) shows liquefaction resistance curves obtained by modeling undrained cyclic DSS tests (σ'_c = 98 kPa) with principal stress rotation. Main observation in the model is the significant increase of liquefaction resistance for K_0 of 2.0. A change in model behaviour is observed for K_0 values lower than 1.0 and values higher than 1.0, leading to higher CSR curves.

As loading continues the model tends to converge to an isotropic stress state. From this state the principal stresses decrease with the same rate to a liquefied state. In Figure 3 the development of the horizontal effective stress over the vertical effective stress (K_0) with different initial K_0 is presented, the trend towards a K_0 of 1.0 is observed. If the initial stress state is already isotropic it remains in this stress state. Converging to an isotropic stress state seems logical, since at an r_u of 1.0 effective stresses are zero and the pore water pressure dominates. The model however already tends to reach this isotropic state before liquefaction occurs influencing the soil behavior. The further the initial stress ratio is away from the isotropic state, the longer the trajectory to an isotropic state and the more cycles are required in the model to reach liquefaction.

To reach the isotropic stress state in the model minor principal effective stresses (σ'_3) initially increase and then decrease towards zero, while major principal effective stresses (σ'_1) continuously decrease towards zero.

Different model behavior for Ohama Sand and Gaiko Sand is observed for a K_0 of 1.0 with respect to K_0 < 1.0. This type of behavior was also observed by Sawada, et al. (2003) in laboratory tests. Looking into the model behavior the phase from $K_0 \neq 1.0$ conditions to K_0 = 1.0 conditions has relatively more influence on the resistance for Ohama Sand than for Gaiko Sand, because the isotropic state is reached earlier for the Gaiko Sand. The gradient of the decreasing effective stresses in the isotropic state is smaller for the Gaiko Sand so the second phase becomes dominant. Reason for this difference is linked to a difference in ratio between k^p_G and fac_{hard} in combination with the corresponding difference in loading level in the element test between both sands, leading to a difference in development of the stress state. In Figure 3 a convex curve is observed for Ohama Sand, while the curve for Gaiko Sand is concave, indicating the difference in stress development.

In an undrained cyclic TX test, anisotropic loading conditions are imposed by imposing a difference in magnitude of the principal stresses, which is identical to imposing initial static shear stresses. A value for K_0 is therefore directly linked to a value of α. For effects of varying K_0 in undrained cyclic TX tests reference is made to section 3.2.3 for effects of initial static shear stresses.

3.2.3 Effects of initial static shear stress (α)

Seed (1983) introduced a K_α-value (= CRR_α / $CRR_{\alpha=0}$) to account for the effects of initial static shear stresses on liquefaction potential depending on the relative density and dilatancy. For the considered sands (Table 1) and stress states (K_0 = 0.50 for DSS and K_0 = 1.0 for TX, σ'_c = 98 kPa and α ranges from 0.00 to 0.20) the liquefaction potential should show minor decrease in CSR for increasing initial static shear stresses according to Seed (1983). For increasing α the CSR rapidly decreases in an undrained cyclic DSS test. The liquefaction resistance is underestimated compared to empirical relationships,

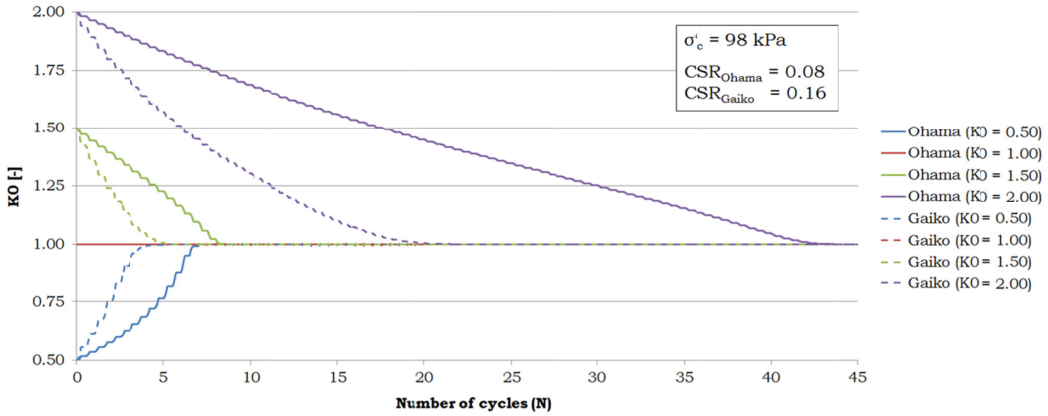

Figure 3. Development K_0 in an undrained cyclic DSS test for both sands for different initial K_0 and loading levels

which is explained by the fact that failure occurs due to flow failure where the shear stress already exceeds the decreasing shear strength of the soil before reaching zero effective stresses. This behaviour is not well captured in the model. In order to fit the K_α obtained from the UBC3D-PLM model with empirical relationships for DSS test, the fac_{hard} and K^p_G are increased. The higher α the larger fac_{hard} and K^p_G to slow down the excess pore pressure generation and to compensate for the underestimation of the liquefaction resistance.

The liquefaction resistance in undrained cyclic TX tests initially increases for low α values but decreases for increasing α as presented in Figure 2(B.). The UBC3D-PLM model underestimates the soil resistance, but to less extent than for DSS tests. The fac_{hard} and k^p_G are increased to fit the K_α, but less compensation is required.

4 AKITA PORT

4.1 Field observations

The well-documented case history of Akita Port is evaluated using a numerical analysis, where two anchored quay walls at Ohama No.1 Wharf and Ohama No.2 Wharf were subject to the Nihonkai Chubu Earthquake in 1983 (Iai 1993). Both anchored quay walls had similar cross sections, however the earthquake with a peak ground acceleration (PGA) of 0.24 g caused severe damage to the quay wall at Ohama No.2 Wharf, see Figure 4, while no damage was observed to the quay wall at Ohama No.1. Sand boils were observed at Ohama No.2 Wharf, while at Ohama No.1 Wharf no signs of liquefaction were evident. Clearly, the damage was caused by liquefaction in the backfill. In this paper, results of the dynamic analysis of Ohama No.2 Wharf including numerical simulation of liquefaction effects with the UBC3D-PLM model for the backfill material are presented.

During the earthquake the top of the anchored quay wall at Ohama No.2 Wharf moved about 1.1 to 1.8 meters towards the sea and experienced a maximum vertical settlement of 1.3 meters. The displacements at the top are associated with those of the anchor piles, which were pulled towards the sea, presumably due to reduced resistance of the liquefied backfill. Cracks in the sheet pile were observed halfway the retaining height at -6.0 m and at 2.2 meters below the sea bottom (-12.2 m) (Iai 1993).

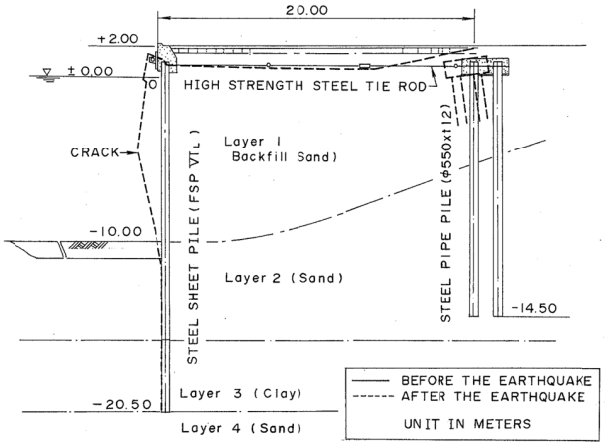

Figure 4. Cross section of the anchored quay wall at Ohama No.2 Wharf (Iai et al. 1993)

4.2 Calibration methodology

It is crucial for UBC3D-PLM model performance to calibrate the model using element tests that properly fit the loading conditions existing in the field, since both the behaviour of the model and the actual soil response in the field are stress path dependent (Kokusho 2015).

The distribution of the lateral earth pressure coefficient (K_0) and initial static shear stresses ratio (α) are determined in the static phase as presented in Figure 1. Based on the distribution of the K_0 distinction is made between active, neutral and passive loading condition. These soil states are subsequently linked to the loading conditions in typical element tests, where an active condition corresponds to the loading condition in an

undrained cyclic triaxial lateral extension test, a neutral condition to the loading conditions in an undrained cyclic direct simple shear test and the passive condition to the loading conditions in an undrained cyclic triaxial lateral compression test. The distribution of the static shear stress ratio (α) is used to determine the initial static shear stress conditions in the element test. Combining both distributions (K_0 and α) translated to element tests leads to the zoning as presented in Figure 5.

The performance of the UBC3D-PLM model is evaluated for both undrained cyclic direct simple shear tests and undrained cyclic triaxial tests for different initial conditions and loading levels. Adjustments to model parameters K^p_G and fac_{hard} are suggested to the initial parameter set depending on the type of element test and initial conditions to improve the model performance for specific loading conditions and sand type. Since zones are defined around the structure corresponding to loading conditions of these typical element tests with known initial conditions, the model of the system can be calibrated locally for each zone based on the knowledge of the performance of the model for the element tests. In Figure 6 the zones defined in the finite element around the anchored quay wall are presented. Each soil zone has a unique material parameter set calibrated for the loading conditions in that zone. To prevent numerical issues as a result of the presence of initial static shear stresses a post liquefaction factor (fac_{post}) of 1.0 is adopted in all model parameter sets.

4.3 Numerical modeling

The seismic response of the typical cross section of the anchored quay wall at Ohama No.2 Wharf is analysed by dynamic nonlinear time history analysis using PLAXIS 2D software. For the upper two soil layers the UBC3D-PLM model is adopted, with model parameters as presented in Table 1 and zone specific calibrated K^p_G and fac_{hard}. The HSsmall constitutive model is assigned to other soil layers, as these are considered to be non-liquefiable. The model parameters are presented in Table 2, for sands based on relationships by Brinkgreve et al. (2010).

Both the sheet pile wall and the anchor wall are modeled as elastic plate elements. Interface elements are defined connecting the walls to the soil mesh. The connecting tie-rod is modeled as a node-to-node anchor (elastic spring) with an out of plane spacing of 2.0 meters.

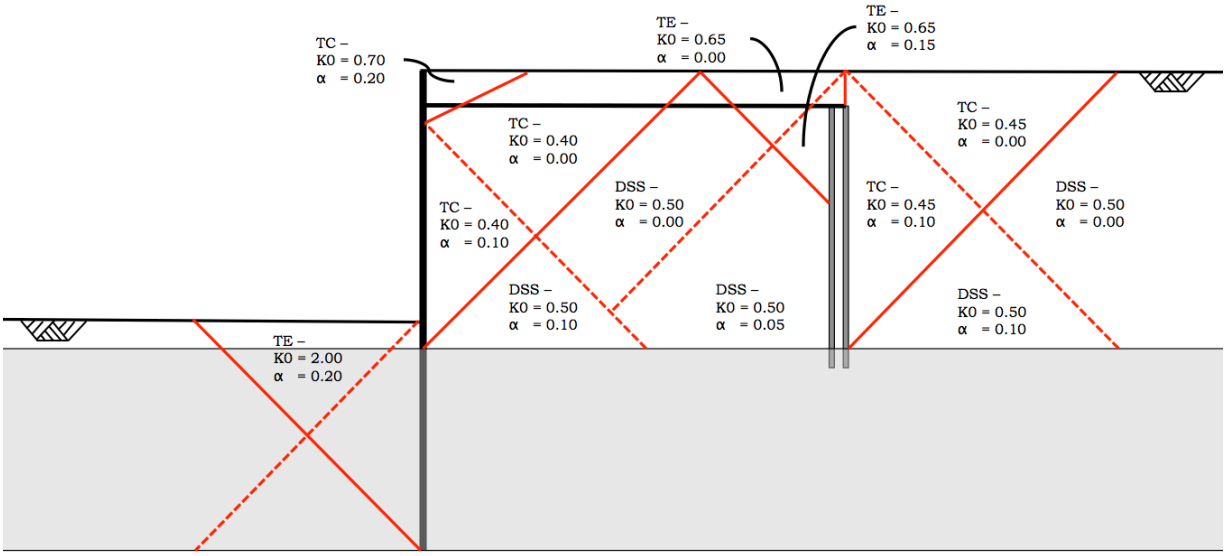

Figure 5. Overview element tests with initial conditions corresponding to existing loading conditions in the field

Table 2. Model parameters HSsmall model for static soil behavior and dynamic soil behavior of non-liquefiable layers

Layer [-]		D_r [%]	$E_{50,ref}$ [kPa]	$E_{oed,ref}$ [kPa]	$E_{ur,ref}$ [kPa]	m [-]	$K_{0,nc}$ [-]	R_F [-]	$G_{0,ref}$ [kPa]	$\gamma_{0.7}$ [-]
1	Ohama Sand	40	2.40E4	2.40E4	4.80E4	0.58	0.50	0.95	8.72E4	3.60E-4
2	Gaiko Sand	60	3.60E4	3.60E4	7.20E4	0.51	0.50	0.93	10.08E4	1.60E-4
3	Sand	85	5.10E4	5.10E4	10.02E4	0.43	0.36	0.89	11.76E4	1.40E-4
4	Clay	\	2.00E4	2.00E4	4.00E4	0.55	0.54	0.92	7.50E4	1.65E-4
5	Sand	65	2.70E4	2.70E4	5.40E4	0.56	0.46	0.94	9.06E4	1.60E-4
6	Sand	70	4.20E4	4.20E4	8.40E4	0,48	0.40	0.91	10.76E4	1.40E-4

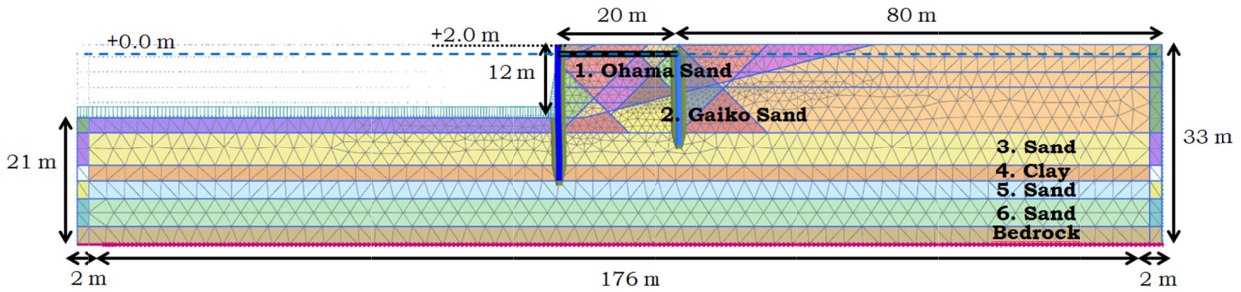

Figure 6. Finite element mesh with indication of dimensions of the model and soil layers

The time motion of the acceleration is imposed at the base of the model as a line displacement with a dynamic multiplier. With a site response analysis of a 1D soil column the damping characteristics of the model for the different soil layers are calibrated prior to the dynamic analysis of the system. Rayleigh damping (1.25% in range of 1.6 - 3.0 Hz) is added to the structures and the soil, to avoid spurious oscillations at small deformations and damp high frequency motions. At the bottom a compliant base boundary is applied and a stiff bedrock layer is modeled to correctly introduce the seismic wave. At both outer sides of the model, free-field boundary columns are applied to model the interaction with the free-field motion and to prevent spurious wave reflections. Soil columns having equivalent strength and stiffness parameters but with drained conditions are adopted at both outer sides of the model to prevent complete loss of support at the boundaries. In Figure 6 the finite element model with mesh and main characteristics is presented.

4.4 Results

In Figure 7 the horizontal displacement of the top of the sheet pile wall in time is presented. The contour lines of the horizontal displacement are presented in Figure 8(A.). As is shown in these figures the calculated residual horizontal displacements of the top of the wall are satisfactorily reproduced. The quay wall deforms significantly in the horizontal direction at the moment the soil reaches the liquefaction criterion at 13 seconds.

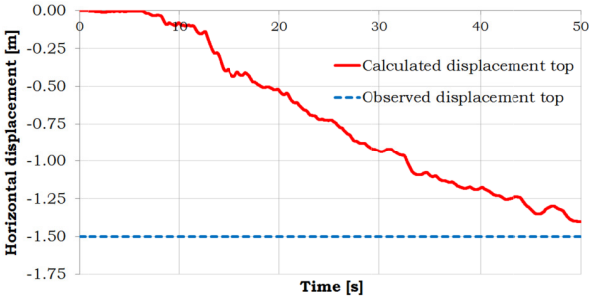

Figure 7. Horizontal displacement of the top of the sheet pile in time

The failure behaviour in the model is in good agreement with the observed failure behaviour, where the sheet pile wall moved forward due to loss of support of the anchor wall. Horizontal movement in time of the sheet pile at the anchor connection shows the same trend as the horizontal movement of the anchor wall.

Concerning the development of excess pore pressures around the structure the results are also satisfactory, see Figure 8(B.). A zone with significantly lower, even locally negative, excess pore pressures is found right behind the sheet pile wall and the anchor wall, while large scale liquefaction is observed in soil layers at some distance from the wall. These observations support conclusions drawn by Brinkgreve et al. (2013) and Souliotis et al. (2016) based on analysis of a case-history of a gravity based quay wall.

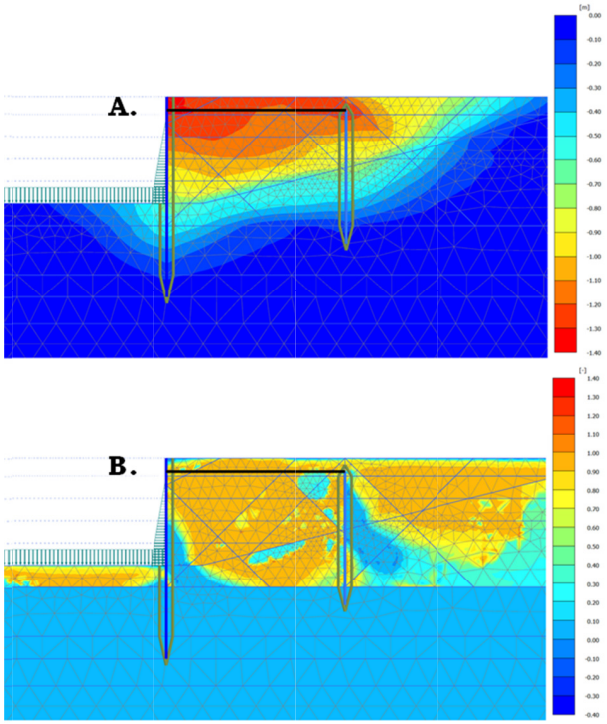

Figure 8. Contours of (A.) the horizontal displacement and (B.) the excess pore pressure ratio at the end of the Nihonkai Chubu Earthquake

5 CONCLUSIONS

This paper presented the capability of the UBC3D-PLM soil constitutive model for predicting the seismic response of an anchored quay wall including liquefaction effects. It is also highlighted that the pseudo-static Mononobe-Okabe methods including corrections for liquefaction effects are concluded to yield a poor fit to the observed behaviour. This study investigates the capabilities of the model to reproduce experimental data of element tests for varying initial stress states and loading conditions. Model parameters obtained with correlations by Beaty & Byrne (2011) and Makra (2013) and Souliotis & Gerolymos (2016) did not provide accurate results for the considered types of sand. Targeted adjustments to the model parameters are proposed leading to reasonable fit of the amount of cycles to liquefaction predicted by the model with experimental data and empirical relationships for different initial stress states and loading conditions. Calibrating the model for these element tests with specific initial stress states is crucial for accurate prediction of the liquefaction potential, in particular, for purpose of the new proposed calibration method.

The case history of an anchored quay wall in Akita Port that suffered severe damage and outward horizontal displacement during the Nihonkai Chubu Earthquake in 1983 as a result of the occurrence of liquefaction in the backfill has been analysed by means of a numerical simulation using the UBC3D-PLM. Using the proposed methodology with locally calibrated zones based on insights in the model behaviour to liquefaction for different stress states, satisfactory results were found. Observed failure behaviour and residual displacement are in reasonable agreement with observations in the field and insight is obtained in the development of excess pore pressures, showing the validity of the proposed methodology of locally calibration of the model.

6 REFERENCES

Beaty, M. and Byrne P. 1998. An effective stress model for redicting liquefaction behaviour of sand, *Geotechnical Earthquake Engineering and Soil Dynamics III*, ASCE, Geotechnical Special Publication No.75, 1:766–777.

Beaty M and Byrne P. 2011. UBCSAND constitutive model, Version 904aR., *Itasca UDM Web Site*, pp. 69.

Brinkgreve, R.B.J., Engin, E., Engin, H.K. 2010. Validation of empirical formulas to derive model parameters for sands. In T. Benz, S. Nordal (eds.), *7th European Conference Numerical Methods in Geotechnical Engineering*, NUMGE, Trodheim, volume 1, pp. 137-174.

Drucker, D.C. and Prager W. 1952. Soil mechanics and plastic analysis for limit design, *Quart. Appl. Math.*, Vol. 9, pp. 381-389.

Galavi, V., Petalas, A., Brinkgreve, R.B.J. 2013. Finite element modeling of seismic liquefaction in soils, *Geotechnical Engineering Journal of the SEAGS & AGSSEA*, Vol. 44, No. 3, pp. 55-64.

Gazetas, G., Garini, E., Zafeirakos, A. 2015. Seismic Analysis of Anchored Sheet-Pile Walls: Are we Over-designing?. *6th International Conference on Earthquake Geotechnical Engineering*, Christchurch, New Zealand

Iai, S. and Kameoka, T. 1993. Finite element analysis of earthquake induced damage to anchored sheet pile quay walls, *Soils and Foundations*, Japanese Society of Soil Mechanics and Foundation Engineering, Vol. 33, No. 1, 71-91

Kokusho, T. 2015. Liquefaction Research by Laboratory Tests versus In Situ Behavior. *6th International Conference on Earthquake Geotechnical Engineering,* Christchurch, New Zealand

Makra, A. 2013. Evaluation of the UBC3D-PLM constitutive model for prediction of earthquake induced liquefaction on embankment dams, MSc Thesis, TU Delft.

Mononobe, N. and Matsuo, H. 1929. On the determination of earth pressures during earthquakes. *Proceedings, World Engineering Congress*.

Okabe, S. 1926. General theory of earth pressures. Technical report, *Journal of the Japan Society of Civil Engineering*.

Rowe, P.W. 1962. The stress-dilatancy relation for static equilibrium of an assembly of particles in contact. *Proc. of the Royal Society of London, Mathematical and Physical Sciences*, Series A, Vol. 269, pp. 500-557.

Sawada, S., Takeshima, Y., Mikami, T. 2003. Effect of K_0-condition on liquefaction characteristics of saturated sand, *Deformation Characteristics of Geomaterials*, *Proceedings of the Third International Symposium on Deformation Characteristics of Geomaterials*, Swets & Zeitlinger B.V. Lyon, France

Seed, H.B. 1983. Earthquake resistant design of earth dams. In Proc., *Symposium on Seismic Design of Embankments and Caverns*, ASCE, Pennsylvania, New York, pp. 41-64.

Skempton, A.W. 1986. Standard penetration test procedures and the effects in sands of overburden pressure, relative density, particle size, aging and overconsolidation. *Geotechnique*, Volume 36 Issue 3, pp. 425-447

Souliotis, C. and Gerolymos, N. 2016. Seismic Analysis of Quay Wall in Liquefiable Soil with the UBC3D- PLM Constitutive Model: Calibration Methodology and Validation. *1st International Conference on Natural Hazards & Infrastructure*, Chania, Greece

Ziotopoulou, K., Maharjan, M., Boulanger, R.W., Beaty, M.H., Armstrong, R.J., Takahashi, A. 2014. *Constitutive modelling of liquefaction effects in sloping ground. Tenth U.S. National Conference on Earthquake Engineering*, Frontiers of Earthquake Engineering, Anchorage, Alaska